Nonlinear seismic modeling of reinforced concrete cores including torsion

by

Kevin Pelletier and Pierre Léger

Department of Civil, Geological and Mining Engineering
École Polytechnique
P.O. Box 6079, Station Centre-Ville
Montreal, Canada H3C 3A7

Corresponding author:
Pierre Léger
Phone: (514) 340-4711 (3712)
Fax: (514) 340-5881
Email: pierre.leger@polymtl.ca

Paper No. *ENGSTRUCT-D-15-01033R3* (Revised R3)
submitted for review and possible publication in
ENGINEERING STRUCTURES

SEPTEMBER 23, 2016

Nonlinear seismic modeling of reinforced concrete cores including torsion

Kevin Pelletier and Pierre Léger

Abstract: Reinforced concrete (RC) cores are used in many residential multi-story buildings as the primary seismic force resisting system (SFRS). Due to architectural limitations, these buildings are often torsionally flexible. To assess the effect of torsion on the nonlinear seismic response of RC cores, a wide-column model (WCM) with fiber elements is used. The nonlinear warping and the nonlinear biaxial (P-M_x-M_y) cyclic behaviors of the WCM are validated against experimental results and exhibit excellent agreement. According to modal and linear time history analyses, the model can adequately capture the dynamic characteristics and seismic response of core structures, including torsion. The WCM is then extended to the nonlinear range to perform three-dimensional (3D) time history analyses of a typical RC building structure located in Eastern North America (ENA) that is subjected to high-frequency ground motions. Three different building configurations with increasing torsional flexibility (B=1.7, B=2.1 and B=2.5, according to the current National Building Code of Canada) are studied to investigate the effect of torsion on the seismic behavior. The nonlinear envelopes of key response parameters are similar to the design envelopes obtained from the linear response spectrum analysis of a shell elements model (B=1.7) with proper inelastic force modification factors. Aside from the story torque, the shear and moment demands remain relatively constant, regardless of the torsional flexibility value. The effective shear stiffness must be carefully selected in the WCM to avoid large questionable rotations.

Keywords: torsion, inelastic warping, reinforced concrete, shear walls, cores, fiber elements, nonlinear seismic behavior, wide-column analogy, numerical model.

1. Introduction

Reinforced concrete (RC) buildings are a very popular and cost-effective solution for residential multi-story constructions in Eastern North America (ENA). Planar and non-planar RC shear walls represent the typical seismic force resisting systems (SFRSs) associated with this type of structure. These walls should be located as close as possible to the perimeter of the building to reduce the torsional flexibility of the structure. To minimize the effect of the structural system on the architectural layout, shear walls often act as stairway and elevator shafts in many RC buildings. Commonly known as cores, non-planar shear walls can have many open tubular shapes and are commonly used in residential constructions (Fig. 1). RC cores are usually designed in each orthogonal direction using a linear response spectrum analysis combined with a static torque applied at each story of the building to account for torsional effects (NBCC 2010 [1], ASCE/SEI 7-10 [2]). Therefore, the nonlinear interaction (P-M_x-M_y and V_x-V_y-T) is not explicitly considered in design. The literature on the nonlinear three-dimensional (3D) behavior of reinforced concrete cores subjected to ground motions is very scarce, especially concerning the effect of torsion on the seismic response. To address this issue, 3D nonlinear time history analyses are performed using an efficient wide-column model (WCM) developed in OpenSees [3]. The model can be applied in commercial software using fiber elements. Thus, the two main objectives of this study are the following: (1) to assess the nonlinear torsional response of the WCM when employed to model reinforced concrete U-shaped shear walls (cores) and (2) to provide additional information on the seismic behavior of torsionally flexible buildings subjected to high-frequency ground motions. The content of this paper is organized as follows. First, a literature review on the consideration of torsion in the numerical analysis of RC cores is presented. Next, the WCM is described in detail and is validated against experimental data to

assess its warping behavior. Finally, a typical RC multi-story building located in ENA is subjected to spectrally matched ground motions. Observations from the nonlinear dynamic response of cores are presented, and the principal conclusions are discussed.

2. Consideration of torsion in the numerical analysis of reinforced concrete cores

2.1 NBCC 2010 and ASCE/SEI 7-10 provisions for torsion

When a building is subjected to earthquake loads, significant torsion can be induced based on the eccentricity e_x between the center of rigidity (CR) of the SFRS and the center of mass (CM) where the inertia forces are acting (Fig. 2). In NBCC 2010 and ASCE/SEI 7-10, this concept is defined as inherent torsion. The rotational component of ground motions and the uncertainties related to the position of the CM and the CR caused by an uneven mass distribution and the stiffness variation in the structural system, respectively, induce an additional seismic moment known as accidental torsion. In both Canadian and American design codes, this accidental torsional moment M_{ta} is considered based on an equivalent static force procedure and is computed as follows for each orthogonal direction at each level x:

$$M_{ta} = A_x F_x p_x D_{nx} \tag{1}$$

where A_x is a torsional amplification factor, F_x is the seismic force, p_x is a ratio, and D_{nx} is the dimension of the structure perpendicular to the direction of the applied forces. In NBCC 2010, p_x and A_x are equal to 0.1 and 1.0, respectively. In ASCE/SEI 7-10, p_x is equal to 0.05, and A_x is computed as follows if the structure is assigned to Seismic Design Category C, D, E or F with Type 1a or 1b torsional irregularity (flexible in torsion):

$$1.0 \leq A_x = \left(\frac{\delta_{max}}{1.2\delta_{avg}}\right)^2 \leq 3.0 \tag{2}$$

where δ_{max} is the maximum displacement and δ_{avg} is the average of the displacements at the extreme points of the structure for each orthogonal direction at each level x. These quantities are

72 computed by applying F_x and M_{ta} to the structure, assuming A_x is equal to 1.0. In NBCC 2010,
73 the same procedure is used to compute the parameter B_x:

74 $$B_x = \frac{\delta_{max}}{\delta_{avg}} \quad (3)$$

75 The parameter B defines the torsional sensitivity of a building and is computed as the maximum
76 value of B_x for each level x in each orthogonal direction. This parameter, proposed by Humar et
77 al. [4], is derived from the ratio between the uncoupled torsional and translational frequencies:

78 $$\Omega_R = \frac{\omega_\theta}{\omega_y} \quad (4)$$

79 Buildings can be considered torsionally flexible when this ratio is smaller than one [4].
80 According to the Canadian standard, a building is considered torsionally irregular when B is
81 greater than 1.7, whereas this limit is equal to 1.2 in ASCE/SEI 7-10. In the American standard,
82 there is an additional category for extreme torsional irregularities when B_x is greater than 1.4. In
83 this paper, the NBCC 2010 limit is used to classify torsional irregularities because the building
84 from the case study is designed in accordance with the Canadian standards.

85 *2.2 Torsional behavior of reinforced concrete cores*

86 Both planar shear walls and RC cores carry shear forces and bending moments when the
87 structure is subjected to lateral loads. However, the torsional resisting mechanism is significantly
88 different between planar shear walls and cores. For the former, torsion is resisted by developing
89 shear forces inversely proportional to the lever of arm between the CR and the position of each
90 planar shear wall. For the latter, the amount of torsion resisted by the cores is related not to their
91 lever arm but rather to their torsional stiffness relative to the total torsional stiffness of the
92 structural system. Thus, RC cores in buildings without planar shear walls can be submitted to
93 large torsional loads because they provide the principal torsional stiffness of the structure. For

such cases, the warping component of torsion can induce significant normal stresses at the base of cores, which can be of similar magnitude as the bending stresses [5]. These normal stresses are proportional to the applied torque at the shear center of the cross-section. Therefore, warping can affect the yielding of vertical reinforcement bars in the plastic hinge region of capacity-designed cores. The warping stiffness of cores is related to the amount of axial restraint, which can be influenced by boundary conditions, coupling beams and slab-column interaction. Foundations are often assumed as rigid and can restrain almost completely warping deformations at the base of cores. Similarly to coupling beams, the out-of-plane bending stiffness of the slab can also offer axial restraint, resulting in additional bending and shear forces. These forces induced in the slab have to be considered in design, especially near the openings of cores [6]. This stiffening effect is enhanced by the presence of peripheral columns supporting the slab. Coull and Chee [7] studied various slab support conditions, from free edges (no columns) to simply supported, to assess the effects of these columns on the warping stiffness of cores. They found that the slab-column interaction can significantly increase the stiffness of the system compared to the free edge configuration. Thus, the axial restraint may have an effect on the behavior of RC cores and therefore, it must be properly accounted for in numerical models.

2.3 Modeling strategies for reinforced concrete cores

If the cores were to be completely closed, it would be possible to model these structures with only beam elements located at the shear center of the cross-section because the warping behavior could be considered negligible [5]. In that case, the Saint-Venant stiffness would provide almost all of the resistance to torsion. However, in addition to their principal structural role, RC cores are often used as stairways or elevator shafts; thus, openings are needed for proper accessibility. Such openings significantly lower the torsional stiffness of cores, which invalidates the

117 negligible warping assumption. Thus, classical beam elements cannot be used because there is no
118 degree of freedom (DOF) associated with warping displacements. To address this issue, Stafford-
119 Smith and Taranath [6] derived the beam element stiffness matrix associated with a 7^{th} DOF per
120 node representing warping and its corresponding force, known as the bimoment. However, this
121 closed-form solution is generally unavailable in structural analysis programs and cannot
122 represent the spread of plasticity for composite sections such as reinforced concrete. Mainly
123 intended for linear static analyses, Stafford-Smith and Coull [5] proposed an alternative to this
124 closed-form solution known as the two-column analogy. Preliminary linear modal analyses by
125 the authors of the current study led them to believe that this analogy is inadequate for dynamic
126 analyses. According to the participating modal mass ratios, the torsional modes of vibration
127 cannot be captured adequately. Furthermore, both alternatives require knowledge of warping
128 theory to compute the sectorial properties of RC cores [5]. These drawbacks might explain the
129 limited applicability of these alternatives by design offices and for research purposes.
130 Initially developed for planar shear walls, the wide-column analogy, also known as the
131 equivalent frame method [8]-[9], was extended to the elastic analysis of cores by Stafford-Smith
132 and Abate [10]. Such wide-column models (WCMs) can account for both bending and warping
133 behaviors when the structure is submitted to eccentric forces. In the initial approach, beam
134 elements with equivalent mechanical properties are located at the centroid of the wall, and rigid
135 links are added to represent the wall width (Fig. 3). Based on this concept, Stafford-Smith and
136 Abate [10] divided the structure into planar subdivisions called frame modules. Multiple types of
137 modules that could be used to avoid the interference between the shear and moment behavior
138 were proposed [11]. However, negative properties are sometimes required for these modules
139 depending on the geometry of the wall. Having negative values in the stiffness matrix can lead to

convergence issues, especially for nonlinear analyses. Instead of employing these modules, Beyer et al. [12] developed an inelastic wide-column model with fiber beam elements to simulate the cyclic behavior of RC cores submitted to biaxial loading histories [13]. The spread of plasticity and the interaction between moments and axial forces can be considered with such elements. In this model, the fiber beams are located at the centroid of each planar segment of the cross-section and are attached together with rigid links to enforce a uniform motion of the structure. To allow warping, these links have a finite Saint-Venant torsional stiffness value. Stafford-Smith and Girgis [14] observed that WCMs suffer from additional displacements and stresses, especially when employed to model core structures. Instead of a continuous shear flow, shear forces are concentrated at the rigid links of the WCM, inducing purely artificial flexure known as "parasitic moments". As illustrated in Fig. 4, the shear displacement Δ_S is the sum of Δ_{SF} and Δ_{PM} caused by shear forces and parasitic moments, respectively [15]. Therefore, the model appears to be more flexible than it really is due to Δ_{PM}. For walls where the behavior is dominated by bending, the additional shear displacements induced by parasitic moments can be considered to be negligible [14]. However, this is not the case for structures with large shear forces such as cores subjected to torsion. To reduce the effect of these moments, Stafford-Smith and Girgis [14] recommend restraining the rigid links spacing to one-fifth of the wall's total height. According to Beyer et al. [12], the shear span should be used instead of the overall height of the structure, and the rigid links spacing should not exceed 50% of the smallest cross-section dimension of the wall. These limits are modeling guidelines rather than strict rules and are intended to ensure the adequate behavior of the WCM.

3. Description of the wide-column model

Beyer et al. [12] showed that an inelastic wide-column model (WCM) with fiber beam-column elements can represent the behavior of RC cores subjected to cyclic biaxial flexural loadings with sufficient accuracy. During their experiment, the RC core was not subjected to significant torsion because the wall head was restrained from twisting by the actuators [13]. Therefore, the accuracy of the WCM for torsional loads could not be assessed, especially in terms of the nonlinear warping behavior. Thus, the torsional response of the WCM proposed by Beyer et al. [12] is assed in this study, especially concerning the inelastic warping behavior. Based on the module concept adopted by Stafford-Smith and Abate [10], the possibility of using more than three modules is also studied herein and is validated against experimental data.

3.1. Description of the WCM

When using the space truss analogy, it is assumed that the shear forces are carried by concrete struts and steel ties when an RC structure is loaded in torsion. The truss angle between struts and ties is approximately 45°, depending on the magnitude of the axial force applied to the structure. This truss action mechanism cannot be properly accounted for in the WCM because only one fiber beam-column per flange is used. Therefore, the shear forces are carried along the only beam-column element available, resulting in a stiffer model in torsion. To address this issue, one could divide the cross-section into m subdivisions called modules (i.e., m=6 in Fig. 5). This enables a better representation of the behavior of RC structures loaded in torsion. According to the division scheme presented in Fig. 5b, the number of modules m is a multiple of three for U-shaped cores. The modules could also be removed to model openings, assuming that enough modules are used to allow proper force redistribution in the structure. However, more research work is needed to assess the performance of the WCM for RC structures with openings. To

represent the axial-moment interaction of the section (P-M_x-M_y), displacement-based fiber beam-columns are located at the centroid of each module. In the WCM developed in OpenSees [3], these beam-columns have no torsional stiffness [12] and therefore a small value corresponding to 10% of the elastic Saint-Venant stiffness is assigned. The nonlinear constitutive laws used for concrete fibers follow the modified Kent and Park model (*Concrete02* in OS) [16]. For reinforcement steel, the Giuffré-Menegetto-Pinto hysteretic model with default parameters (*Steel02* in OS) [3] or a bilinear hardening curve is used, depending on whether cyclic analyses are required. Rigid links are needed to bind the columns together to allow for the uniform motion of the structure. These links are rigid axially, in shear and for in-plane bending, whereas their Saint-Venant torsional stiffness has a finite value computed with gross section dimensions (Fig. 5a). In parametric analyses, this value can be changed using the F_{JL} factor as indicated in section 3.2, where a specific F_{JL} factor is recommended. In Fig. 5a, the local axes of the rigid links are indicated with the subscript L. The warping stiffness is inherently considered in the formulation of the wide-column analogy by allowing axial out-of-plane deformation (the cross-section is allowed to not remain plane). Out-of-plane bending flexibility of the rigid links is added to allow local out-of-plane deformations, which can be important for torsionally sensitive structures such as RC cores. This out-of-plane stiffness is computed using gross section properties. To avoid excessive parasitic moments, it is recommended that the rigid links spacing should not exceed either $1/5^{th}$ of the total height H of the structure [14] or 50% of the smallest cross-sectional dimension, whichever is smallest [12]. This limit should be decreased to 30% for the WCM when multiple modules are used, as it will be shown later. RC shear walls can undergo large shear deformations in the plastic hinge region during an earthquake because the ratio of shear to bending deformation remains constant in the inelastic regime if the shear transfer mechanism is

not deteriorated [17]. This in-plane shear flexibility is accounted for using zero-length elements at half-distance of the rigid links spacing, and two fiber beam-column elements are modeled between each link as recommended by Beyer et al. [12]. The effective shear stiffness is computed using gross section elastic properties according to the following equation:

$$G_{in-plane} = G_c \frac{5}{6} \frac{h_m t_m}{S_L} \quad (5)$$

where h_m and t_m are the module height and thickness, S_L is the rigid links spacing, and G_c is the concrete shear modulus. In theory, the 5/6 factor is valid only if one module per flange is used because it transforms the shear area with the exact parabolic shear stress distribution into one with a constant shear stress distribution. For the sake of simplicity, this reduction factor is used regardless the number of modules. The out-of-plane effective shear stiffness of the modules assigned to the zero-length elements is assumed to be 25% of the in-plane value [12].

3.2. Validation case 1: pure torsion

To validate the WCM hysteretic behavior, experimental data of RC cores subjected to cyclic biaxial flexural loading including torsion are needed. To the best of the authors' knowledge, such data are currently unavailable. Therefore, the WCM is first validated against the Krpan and Collins [18] test of a thin-walled RC channel beam loaded in pure torsion at midspan. The details of experimental setup, instrumentation and measured responses are described in reference [18]. The warping behavior of this beam can be considered similar to RC cores subjected to torsion because those are usually assumed to be thin walled. This test is appropriate for validating the accuracy of the WCM in monotonically increasing pure torsion. The 6400-mm-long channel beam was torsionally restrained at both ends using rigid concrete blocks and was heavily reinforced with #2 stirrups at 76 mm c/c to avoid brittle shear failures. The 75-mm-thick cross-section had a width of 840 mm and a depth of 650 mm and was reinforced with #5 steel bars

230 detailed to resist high axial forces due to warping. A 200-mm-thick rigid diaphragm was located
231 at midspan where the torque was applied using a steel loading frame. This frame was loaded with
232 two equal and opposite forces applied at each end using steel rods. During the test, the
233 longitudinal reinforcements first yielded due to warping at a torque T of approximately 190 kN-
234 m, whereas the stirrups yielded at approximately 240 kN-m (points 1 and 3, respectively, in Fig.
235 6). The first 203-mm-long strain gauges were installed at approximately 150 mm from the end
236 blocks, meaning that the reinforcements had most likely yielded before the assumed
237 experimental yield point. This yield point is identified when at least one reinforcing bar reaches
238 the yield strain. For comparison purposes, the same definition is applied to numerical simulations
239 considering a representative yield reinforcement length of 100 mm (half of the strain gauge
240 length) for this study.
241 The numerical simulations are performed using OpenSees (v2.4.4). For comparison purposes, a
242 detailed ABAQUS (v6.11-2) [19] nonlinear model is also developed because shear behavior
243 caused by torsion can be difficult to properly capture. For both models, only one-half of the
244 structure (3200 mm) is modeled due to symmetry. Longitudinal displacements along the global
245 Z-axis and rotations about the global X- and Y-axes are restrained at the free end (see Fig. 7 for
246 axis orientations). The same constitutive nonlinear material laws used for the WCM are specified
247 for the ABAQUS nonlinear model. Table 1 presents concrete values computed according to
248 CSA/A23.3-14 [20] and the steel properties used for the numerical simulations. To enhance the
249 numerical stability, a linear post-peak descending curve for concrete in tension is defined from
250 the maximum tensile strength to a strain value of 0.002, which is approximately the yield strain
251 of reinforcements. No tension stiffening prior to cracking is assumed for concrete.
252

Table 1. Material properties (MPa)

	Unconfined concrete			Confined concrete			#5 / D12 rebars			#2 / D6 rebars		
	f'_c	f_t	E_c	f'_{cc}	f_{tc}	E_{cc}	F_y	F_u	E_s	F_y	F_u	E_s
Validation case 1	53.0	4.33	32 450	58.0	4.57	34 275	348	475	194 000	362	490	203 000
*Validation case 2	77.9	5.30	39 717	86.7	5.59	41 898	488	595	200 000	518	681	200 000

*Two similar confined concrete properties were computed according to the stirrup detailing. Only the highest values are shown.

The 3D ABAQUS model consists of eight-node solid elements for concrete with reduced integration and relax stiffness hourglass control. The concrete stress-strain relationship is input in ABAQUS using the concrete damaged plasticity (CDP) model with default parameters. The shape of the hyperbolic flow potential function of the CDP is defined by the dilation angle ψ and the eccentricity ε, which influences the curvature of the function at low confining pressures [19]. To avoid underestimation of the shear resistance of concrete, a dilation angle of 13° and an eccentricity of 90 is specified [21]. The longitudinal reinforcements and stirrups are modeled with three-node truss elements with steel hardening and are assigned an embedded constraint to ensure a monolithic behavior with concrete. To apply the torque, two steel blocks with contact constraints are located at opposite corners of the structure and are loaded with a uniform pressure. These blocks, shown in white in Fig. 7a, represent the loading frame used in the experiment. As depicted in Fig. 6, the ABAQUS model shows very good agreement with the experimental response prior to longitudinal reinforcement yielding. The model appears to be more flexible than the experimental response after this point. To enable the visualization of concrete cracking, the *damageT* variable is defined as the ratio between the current stress state and the tensile strength f'_t of concrete only when the cracking strain is exceeded. Otherwise, it is equal to zero. As illustrated in Fig. 7a, the model exhibits concrete cracked zones rather than discrete cracks because the CDP model is based on the smeared cracks approach. At failure, both

longitudinal reinforcements and stirrups have yielded, as shown in Fig. 7b. The inelastic warping behavior is well captured because the longitudinal reinforcements have yielded in compression where the load is applied, whereas they have yielded in tension at the opposite corners. The stirrups yielding along the entire structure indicates that shear forces were carried by these reinforcing bars when the concrete cracked. Thus, the ABAQUS model exhibits a satisfactory global inelastic response and is able to capture the warping behavior caused by torsion.

Parametric analyses complementary to those presented by Beyer et al. [12] were conducted to assess the sensitivity of the WCM to torsion. Because the rigid links play a crucial role in the model behavior, two main parameters associated to these links, namely, their Saint-Venant stiffness J_L and their spacing S_L, were studied. The adimensional factor F_{JL} in this study corresponds to a proportion of the elastic value of J_L. Fig. 8a shows the J_L sensitivity analysis for three modules (m=3). The torsional stiffness of the rigid links has a significant effect on the behavior, especially for the inelastic portion of the curve. A similar trend is observed when the number of modules is greater than three. Considering their wall test results, where a torsional moment was applied but with no significant rotation due to boundary conditions, Beyer et al. [12] proposed assigning 25% of the elastic Saint-Venant stiffness (F_{JL}=0.25) to the rigid links to consider the inelastic cracking of concrete. They also observed that the biaxial response of the WCM was not very sensitive to the assigned F_{JL} value as long as the rigid links remained torsionally flexible to allow out-of-plane deformations. In contrast, the inelastic warping behavior due to torsion loads is significantly influenced by this parameter, as illustrated in Fig. 8a. To achieve convergence and to prevent numerical instabilities, it is recommended that an F_{JL} value of 25% be specified for loadings as well. The original calibration that was carried out for zero rotation in [12] is shown in fact to be valid when much larger rotational demands is present.

296 The rigid links spacing should not be larger than 325 mm to avoid excessive parasitic moments,
297 which artificially soften the model [12]. However, this proposed limit is not sufficiently
298 restrictive for the WCM when the number of modules is larger than three, as shown in Fig. 8b. A
299 spacing of 200 mm, which corresponds to approximately 30% of the smallest cross-sectional
300 dimension, was needed to achieve convergence and is adopted for this validation case.
301 The sensitivity analyses enabled appropriate parameters that properly captured the inelastic
302 warping behavior of non-planar RC structures to be found. According to Fig. 6, the WCM
303 exhibits excellent agreement with the experimental torsional response regardless of the number
304 of modules, which demonstrates the robustness of the approach. The concrete tension stiffening
305 prior to cracking is not captured because the smeared crack approach is used. Also, the response
306 slightly softens toward the solution as the number of modules increases. The stirrups were not
307 modeled in the WCM, which explains the response discrepancies when the yield point of stirrups
308 is reached. For both WCM and ABAQUS models, the numerical yield point of longitudinal
309 reinforcements is relatively close to the experimental one. The main goal of this validation case
310 was to assess the capabilities of the WCM in simulating the global inelastic response of a RC
311 structure subjected to a torsion load, especially concerning the longitudinal reinforcement
312 yielding caused by warping. The WCM can properly represent such behavior, but it cannot
313 model stirrup yielding and shear failure. Assuming that capacity-designed RC cores are expected
314 to yield in flexure and remain elastic in shear, this is a rather small disadvantage compared to the
315 computational efficiency of the model. For seismically deficient buildings, one could compare
316 the computed elastic shear forces values to the shear capacity of the structure to detect potential
317 shear failure mechanisms. Corrective actions or more sophisticated reinforced concrete
318 constitutive models can then be considered to investigate these potential failure mechanisms.

3.3. Validation case 2: biaxial flexural loading

In addition to the torsional behavior of the WCM, the biaxial flexural cyclic response needs to be validated to ensure a representative numerical model of an RC core submitted to three-dimensional loads. This was done extensively by Beyer et al. [12]. Thus, the objective for this validation case is to determine whether or not the use of multiple modules may improve the response of the model. The TUA specimen of the Beyer et al. [13] experiment is selected to assess the capabilities of the WCM with multiple modules in biaxial flexure. The specimen was a 2720-mm-high RC core fixed in a concrete foundation at its base and had a wall thickness of 150 mm, a width of 1300 mm and a depth of 1050 mm. The distributed and boundary zone reinforcements consisted of D6 and D12 steel bars, respectively. The unconfined concrete compressive strength was 77.9 MPa (see Table 1 for material properties). The core was post-tensioned with an axial force of 780 kN (including self-weight and experimental equipment loads), which was maintained constant during the test to simulate the tributary gravity loads. Three actuators were attached to the 300-mm-thick concrete collar at the top of the core to apply the loading history. The two NS actuators acted in the direction parallel to the flanges with a shear span of 2950 mm. The other one, identified as the EW actuator, acted in the direction parallel to the web, with a shear span of 3350 mm. Fig. 9a presents a view of the experimental setup. As shown in Fig. 9b, the complete loading history consisted of the following cycles for each ductility level in the following order: O-A-B-O (EW direction), O-C-D-O (NS direction), O-E-F-O (diagonal direction) and O-A-G-D-C-H-B-O (sweep motion). For the elastic loading histories (25, 50, 75 and 100% of the predicted yield forces), the sweep cycle was replaced by another diagonal cycle, O-H-G-O.

Aside from the concrete constitutive model and the maximum fiber size of 25 mm, the WCM presented herein is the same as the one used by Beyer et al. [12] labeled as “WCM with state-of-the-art properties”. Beyer et al. [12] showed that better estimates of the shear stiffness of the wall sections led to significantly improved results. Stafford-Smith and Coull [22] indicated that "*In structures that are heavily dependent for their torsional resistance on the torsional stiffness of a core, the vertical warping stresses at the base of the core may be of the same order of magnitude as the bending stresses". B*ecause warping stresses are significantly larger in the corners of U-shaped structures, assigning shear flexibility to the rigid links affects the warping behavior of the WCM. Thus, it was decided not to introduce shear flexibility into the links to avoid an additional modelling parameter to be properly defined and calibrated. In accordance with validation case 1, a value of 25% is specified for F_{JL}. As depicted in Fig. 10, the WCM shows very good agreement with the experimental results and numerical results reported by Beyer et al. [12]. Fig. 10 shows that using more than three modules for the WCM (m=9) slightly improves the numerical response, especially for high ductility levels. However, the convergence was significantly more difficult to achieve. Thus, using more than three modules is not efficient when considering both accuracy and computational time. The WCM has shown excellent agreement with the experimental response for both torsion only (validation case 1) and cyclic biaxial flexural loadings (validation case 2). However, it was not possible to assess the WCM behavior of RC cores for a full cyclic biaxial flexural loading including torsion because such experimental data are currently unavailable. The WCM is believed to represent the behavior of RC cores subjected to three-dimensional inertia forces caused by earthquake loadings reasonably well. Specifying only three modules (m=3) and an F_{JL} value of 25% appears to be adequate to

363 efficiently compute representative results for the seismic analyses of RC buildings, and these
364 parameters are assumed as default values for the following case study.

365 **4. Case study**

366 The calibrated WCM is used for the 3D nonlinear time history analysis of a typical mid-rise
367 reinforced concrete building located in Eastern North America, which is a region subjected to
368 ground motions with high-frequency content (10 Hz). Before performing the nonlinear
369 simulations, the dynamic behavior of the WCM is validated with linear modal and time history
370 analyses. The proposed model is then extended to a nonlinear range and subjected to 12 scaled
371 ground motions in each orthogonal direction for three building configurations (B=1.7 (regular in
372 torsion), B=2.1(moderately sensitive in torsion) and B=2.5 (torsionally sensitive) according to
373 the NBCC 2005 and 2010).

374 *4.1. Description of the selected building*

375 Initially designed in compliance with the NBCC 2005 [23] and the A23.3-04 [24], the selected
376 twelve-story building is 45.0 m high and is founded on class D stiff soil in Montreal (Canada).
377 The total height is 48.65 m if the penthouse on the roof is considered. All dimensions and
378 reinforcement detailing are exhaustively described in reference [25]. Fig. 11 shows the plan view
379 of the building and the material property assumptions. The typical distance between two floors is
380 3.65 m, and the first story height is 4.85 m. The gravity-resisting system consists of 200-mm-
381 thick flat plate slabs supported by 550x550-mm columns. To resist the horizontal forces, two
382 400-mm-thick elevator cores with 900-mm-deep coupling beams are located at the center of the
383 building, which results in a symmetric SFRS. The cores have a height of 48.65 m and provide
384 access to the penthouse on the roof. Distributed 10M vertical bars and four boundary zones
385 (4x25M bars) located at the corners of each core provide the flexural resistance. The coupling

386 beams are reinforced with eight 20M diagonal bars. In the NS direction, the cores are considered
387 as ductile shear walls, and hence, R_d=3.5 and R_o=1.6, which are the force modification and
388 overstrength factors for seismic design in the Canadian code, respectively. In the EW direction,
389 R_d=4.0 and R_o=1.7 because the SFRS is a ductile coupled wall system. According to the linear
390 response spectrum analysis of a shell element model developed in ETABS 2015 [26], the cores
391 satisfy the requirements of the NBCC 2010 and the A23.3-14 if the amount of transverse
392 reinforcements is increased. Thus, the building initially designed according to the NBCC 2005
393 and the A23.3-04 is used because the transverse reinforcements are not modeled in the WCM.
394 The core walls were dimensioned following the capacity design principles, and therefore, these
395 reinforcements should remain mostly elastic during an earthquake.
396 *4.2. OpenSees model*
397 The WCM with three modules (m=3) is used to develop a three-dimensional model of the two
398 cores in OpenSees. The foundations are assumed rigid, and therefore, the nodes at the base are
399 fixed. The high in-plane stiffness of the slab is accounted for with a rigid diaphragm constraint,
400 and the seismic masses are lumped at the master node of every floor. Gravity loads in the cores
401 are distributed in each column of the WCM according to static equilibrium, and P-Δ effects are
402 neglected. Each vertical reinforcement is modeled with fiber elements following the Giuffré-
403 Menegetto-Pinto hysteretic constitutive laws (*Steel02* in OS with default parameters) [3]. The
404 maximum size of the concrete fibers is 100 mm along the core thickness and 200 mm along the
405 wall length. In the boundary zones, this value is decreased to 100 mm because higher strains are
406 expected in these zones. An approximate total of 300 concrete fibers are used to ensure both
407 precision and computational efficiency. The confinement and the nonlinear behavior of concrete
408 is considered according to the modified Kent and Park model [16] (*Concrete02* in OS). The

409 tension stiffening effect is neglected for dynamic analyses because it causes an overestimation of
410 the shear force and moment envelopes [27]. Therefore, a large value is specified in OpenSees for
411 the tension softening modulus to ensure that no residual tensile force can be carried by concrete
412 once it cracks. The coupling beams are also modeled with nonlinear fiber elements. Based on the
413 modeling guidelines proposed by Beyer et al. [12], the rigid links spacing for the typical stories
414 is fixed at 1825 mm, which is half of the story height and corresponds to 57% of the smallest
415 dimensions of the core. Three rigid links are modeled with a spacing of 1617 mm for the lobby
416 because the height is higher than the typical stories. For the linear analyses, the effective in-plane
417 shear stiffness is computed for all stories with 5/6 of the gross shear area, whereas 25% of this
418 value is used for out-of-plane shear stiffness. To account for the amplification of the base shear
419 and the formation of a second plastic hinge in the upper wall region caused by higher modes
420 effects (HMEs), Luu et al. [28] proposed various effective in-plane shear stiffness factors based
421 on parametric studies of shear walls designed according to NBCC 2010 and A23.3-04. For the
422 nonlinear analyses, the 5/6 shear area factor is changed to the recommended values of 50 and
423 20% only for the 1st story and where the second plastic hinge due to HMEs is expected, which
424 corresponds to the 6th, 7th and 8th stories. The effective in-plane shear stiffness factors proposed
425 by Luu et al. [27] were obtained from models with an initial stiffness-proportional Rayleigh
426 damping equal to 1.5% of the critical value. This type of damping may lead to large artificial
427 viscous damping forces [29]. Comparative nonlinear analyses between initial and committed
428 stiffness-proportional damping were performed in OpenSees and showed that these damping
429 forces were not significant for the selected building. Therefore, the initial stiffness-proportional
430 critical Rayleigh damping of 1.5% is adopted for the dynamic analyses to ensure consistency
431 with the derived effective shear stiffness factors. The Rayleigh coefficients are computed

according to the first and sixth modes, which corresponds to a cumulative modal mass ratio of approximately 90%. The OpenSees source code of the WCM model can be found in [30] or by directly contacting the authors.

4.3. Modal analysis

A modal analysis can provide useful information about the dynamic behavior of a structure, including the modes of vibration, the mode shapes and their associated participating modal masses. Assuming that the mass matrix is identical, these modal results can also help assess the similitude between two numerical models representing the same structure. Thus, the WCM is compared to the ETABS elastic shell model developed for the response spectrum analysis. The flexural and shear stiffness reduction factors recommended by the A23.4-04 are specified for both models to account for the cracking of concrete due to the earthquake displacement history. Therefore, a factor of 0.70 is applied to the axial and bending stiffness of the cores. For the coupling beams, 45 and 25% of the shear area and the moment of inertia is used, respectively. However, these factors were not applied to the nonlinear dynamic time history analyses because cracking is directly considered by the nonlinear constitutive concrete hysteric laws. As shown in Table 2, the WCM exhibits excellent agreement with the ETABS model concerning the modal results. Only the first six modes of vibration are shown, but a similar trend can be observed for the higher modes. The parameters U_X and U_Y represent translation in the EW and NS directions, respectively, and R_Z indicates rotation about the vertical Z-axis. As expected for symmetric SFRS, the modes are completely uncoupled. The first mode of vibration is in torsion, which indicates that the building may be torsionally flexible. To assess the coupled behavior of the WCM, the center of mass (CM) was displaced from the center of rigidity (CR) in both numerical models. The coupling between the different modes is also well captured (Table 3). Thus, the

455 WCM should properly represent the dynamic behavior of the cores in time history analyses,

456 especially if torsion is a significant component of the response.

457 Table 2. Periods and participating modal masses (%) (with A23.3-04 stiffness reduction factors)

458 – No mass eccentricity applied

Shell (ETABS)				WCM (OS)				Variation (Shell / WCM)			
T (s)	**U_X**	**U_Y**	**R_Z**	**T (s)**	**U_X**	**U_Y**	**R_Z**	**T (s)**	**U_X**	**U_Y**	**R_Z**
1.92	0	0	77.2	1.89	0	0	78.8	0.98	-	-	1.02
1.85	0	66.52	0.0	1.87	0	66.78	0.0	1.01	-	1.00	-
1.74	72.05	0	0.0	1.68	71.71	0	0.0	0.97	1.00	-	-
0.56	0	0	13.1	0.57	0	0	12.4	1.02	-	-	0.94
0.45	17.19	0	0.0	0.43	17.79	0	0.0	0.96	1.03	-	-
0.33	0	21.44	0.0	0.35	0	21.65	0.0	1.04	-	1.01	-

459

460

461

462

463

464

465 Table 3. Periods and participating modal masses (%) (with A23.3-04 stiffness reduction factors)

466 – 0.1D_{nx} mass eccentricity applied in the EW direction

Shell (ETABS)				WCM (OS)				Variation (Shell / WCM)			
T (s)	**U_X**	**U_Y**	**R_Z**	**T (s)**	**U_X**	**U_Y**	**R_Z**	**T (s)**	**U_X**	**U_Y**	**R_Z**
2.14	0	33.35	40.1	2.12	0	37.58	36.3	0.99	-	1.13	0.91
1.74	72.05	0	0.0	1.68	71.71	0	0.0	0.97	1.00	-	-
1.66	0	33.1	37.1	1.67	0	29.12	42.5	1.00	-	0.88	1.14
0.58	0	2.78	10.8	0.59	0	2.94	9.9	1.02	-	1.06	0.92
0.45	17.19	0	0.0	0.43	17.79	0	0.0	0.96	1.03	-	-
0.32	0	16.79	3.7	0.33	0	15.94	4.1	1.04	-	0.95	1.12

467

468

4.4. Linear time history analysis

Three-dimensional linear time history analyses are performed to assess the dynamic behavior of the WCM subjected to earthquake accelerations and to ensure the robustness of the proposed model for nonlinear simulations. The 12 selected ground motions (GM1 to GM12) from Luu et al. [28] are used for the time history analyses (linear and nonlinear) and are spectrally matched with the NBCC 2010 response spectrum for a class D soil site, which is nearly identical to the NBCC 2005 response spectrum. The 3D linear time history results for the building subjected to ground motion GM1 in the NS direction are presented in Fig. 12 and exhibit excellent agreement. The proposed model can properly represent the linear dynamic behavior of RC cores subjected to ground motions. Thus, the WCM is extended to the nonlinear time history analyses.

4.5. Nonlinear time history analyses

As presented in Table 2, the first mode of vibration of the selected building is torsion, and thus, the torsional component in the dynamic response might be significant. This building can be considered torsionally irregular because B=1.7 according to the NBCC 2010. To assess the effect of torsion, two additional configurations (B=2.1 and B=2.5) are used for the 3D nonlinear time history analyses (Table 4). The configuration for which B=2.5 could be considered as sensitive to torsion whereas B=1.7 is the limit between torsionally regular and irregular buildings according to the Canadian code. To artificially increase the torsional flexibility of the building, the CM is shifted from the CR to provide an inherent mass eccentricity e_x. For each configuration, the accidental torsion is accounted for by moving the CM an additional distance equal to $\pm 0.05 D_{nx}$. The total eccentricity $e_x + 0.05 D_{nx}$ is the only case considered to maximize the torsional solicitation of the building, which yields the maximum force, moment and displacement envelopes. To facilitate an easier interpretation of the results, this total eccentricity is specified as

positive along the X-axis for the NS direction analyses and as negative along the Y-axis for the EW direction analyses. Thus, a positive torsion (counter-clockwise rotation) is always induced when the building is subjected to a positive ground motion displacement according to the axis convention of Fig. 11.

Table 4. Building configurations

	B=1.7	B=2.1	B=2.5
Ω_R	0.66	0.61	0.53
e_x (mm)	0	1 625	3 250
$e_x + 0.05D_{nx}$ (mm)	1 488	3 113	4 738

The combination of the three building configurations and the 12 scaled ground motions applied in each orthogonal direction (EW and NS) yields a total of 72 3D nonlinear time history analyses. The selected transient integrator is the Newmark average acceleration method (γ=1/2 and β=1/4), and the time increment is fixed to 0.005 s. The nonlinear equations of motion are solved with the Newton-Raphson algorithm available in OpenSees. When the convergence is difficult to achieve, the Newton-Raphson with line search algorithm is used. Depending on the earthquake acceleration history, the analysis time is between approximately 20 and 60 minutes using an Intel® i5-2500k@3.30 GHz quad-core processor. The modal analysis for each building configuration was performed before the time history analyses to assess the effect of torsional flexibility on the dynamic response of the structure. As shown in Table 5, the degree of coupling between translation in the NS direction and rotation increases as the building becomes more flexible in torsion, which results in a redistribution of the modal masses. The EW translational modes of vibration are not subject to this coupling effect because the CM eccentricity is defined

along the EW direction. This phenomenon is also observed when the center of mass is shifted from the CR in the NS direction.

Table 5. Periods and participating modal masses (%) for the three building configurations– Mass eccentricity applied in the EW direction

B=1.7				B=2.1				B=2.5			
T (s)	**U_X**	**U_Y**	**R_Z**	**T (s)**	**U_X**	**U_Y**	**R_Z**	**T (s)**	**U_X**	**U_Y**	**R_Z**
1.76	0.0	28.25	46.0	1.88	0.0	35.44	38.5	2.01	0.0	39.71	34.4
1.56	0	39.1	32	1.46	0	31.8	39	1.37	0	27.4	43
1.33	70.4	0	0.0	1.33	70.4	0	0.0	1.33	70.4	0	0.0
0.55	0.0	0.85	16.4	0.57	0.0	3.23	14.2	0.60	0.0	6.19	11.4
0.32	21.5	0	0.0	0.33	0.0	3.68	4.3	0.34	0	0.7	4
0.32	0	16.0	2.1	0.32	21.51	0.0	0.0	0.32	21.51	0.0	0

To assess the effect of the axial restraint of the slab on the dynamic behavior of the cores, a complete shell model of the building, including the slab and the gravity columns, is developed in ETABS 2015. From this model, vertical truss elements are calibrated and added to the WCM to connect the horizontal rigid links together. However, preliminary nonlinear time history analyses showed that no significant difference could be observed when the cores are partially restrained in the vertical direction. Thus, the axial restraint of the slab is neglected in this study. Only the results obtained for the 3D nonlinear time history analyses in the NS direction are presented herein because the results for the EW direction lead to similar conclusions. For comparison purposes, the design envelopes (for B=1.7) obtained from the linear spectrum analysis of the ETABS 2015 shell model including the A23.3-04 stiffness reduction factors are presented. The seismic force modification (R_d=3.5) and overstrength (R_o=1.6) factors are also applied to the spectral results. Another set of design envelopes for shear and torsion, including a dynamic shear amplification factor ϖ_v, is also presented. This factor accounts for inelastic effects of higher

531 modes and was not considered in the initial design of the building because this is a new clause in
532 the A23.4-14 (21.5.2.2.7). A static torque is applied at each story of the building in the shell
533 model to include accidental torsion. Fig. 13 shows the response of the building to the GM1
534 earthquake. According to the top CM displacement and rotation time histories, the fundamental
535 period of vibration in flexure and in torsion is approximately 2.25 s. A small delay can be
536 perceived between the translational and rotational displacement peaks in the forced vibration
537 response of the building, as noticed in the other ground motion time histories. The effect of the
538 CM eccentricity on the base torque can be clearly observed, whereas the shear and moment at the
539 base of the building remain similar regardless of the value of B. This phenomenon is due to the
540 increased degree of coupling between the translational and rotation modes. For the same
541 displacement in translation, a larger rotation is induced as the CM moves farther from the CR for
542 higher B values. In the NS direction, the probable plastic moment M_p of each core is 60.7 MN-
543 m, for an approximate total of 120 MN-m. The M_p value is computed considering steel strain
544 hardening (f_s=1.25F_y) and by assuming resistance factors of 1.00 (ϕ_c=ϕ_s=1.00). Fig. 13e clearly
545 shows that the total moment at the base of the cores where the plastic hinge is expected is limited
546 to approximately 120 MN-m, which corresponds to their probable flexural capacity.
547 In Fig. 14 and Fig. 15, the design envelopes are obtained from the NBCC 2005 linear response
548 spectrum analysis of the designed building (B=1.7). The envelopes including the dynamic shear
549 amplification factor ϖ_v are labeled DSA. According to Fig. 14, the design rotations are
550 conservative. The rotational demand is significantly increased for increased B because the
551 building is more flexible in torsion. Assuming the small displacements hypothesis, the rotational
552 drift for each story *i* is computed according to the following equation:

553 $$\delta_{\theta i} = (\theta_i - \theta_{i-1}) \frac{d_i}{h_i} \quad (6)$$

554 where θ_i is the CM rotation, h_i is the story height, and d_i is the shortest perpendicular distance
555 from the CM to the edge of the floor. According to the building configurations and the axis
556 convention, a positive rotation causes a positive translation on the short side of the building,
557 which is defined as the nearest floor edge located perpendicularly from the center of mass. For
558 this building, the largest total drift is always on the short side because the relative contribution of
559 rotation to the total drift is small compared to the translational displacement contribution. As
560 shown in Fig. 14d, the rotational drift is considerably higher for the 6th, 7th and 8th stories because
561 a low effective shear stiffness equal to 20% is assigned to these stories, as suggested by Luu et
562 al. [28]. These factors were specified in the model to account for higher modes effects in the
563 upper part of the cores. In contrast, no noticeable effect can be observed for the translational drift
564 because flexure is the primary deformation mechanism. Thus, the effective shear stiffness must
565 be properly selected if the cores are expected to undergo large rotational demands.
566 The force and moment envelopes are similar for both cores; thus, only the results for the east
567 core are presented in Fig. 15. The design moment envelope is much lower than the dynamic
568 response because the factored flexural resistance M_r of the cores was significantly larger (51.1
569 MN-m) than the factored design moment M_f (27.6 MN-m). According to the capacity design
570 principle, the design shear force envelope is amplified (ϖ_v=1.47), as suggested in A23.3-14
571 (clause 21.5.2.2.7), to prevent brittle shear failure and to account for the higher modes effects
572 (DSA envelopes in Fig. 15). The design story torque is amplified as well because it is induced by
573 shear forces. The DSA envelopes clearly show that the dynamic shear amplification factor newly
574 introduced in A23.3-14 allows a more realistic seismic shear force demand to be obtained
575 compared to nonlinear time history results (B=1.7). The core shear and moment from the
576 nonlinear time histories remain relatively constant regardless the value of B. In contrast, the

577 torsional demand becomes significantly larger when the building is more flexible in torsion
578 because the CM eccentricity is larger. The effect of the higher modes on the story shear
579 distribution can be observed in the upper part of the cores, and the torsion envelope is altered in a
580 similar manner. The building design envelopes for B=1.7, which was the initial building
581 configuration used to design the steel reinforcement, show very good agreement with the
582 nonlinear time history envelopes.
583 The three-dimensional nonlinear time history analyses showed a small delay between the
584 translation and rotation peaks of the forced vibration response of the building. To rationally
585 investigate this observation, a cross-correlation study comparing the translational and rotational
586 behavior of the building was conducted. Cross-correlation is a tool used in signal post-processing
587 to determine whether two delayed signals are correlated. For each ground motion applied to the
588 building in each direction (EW and NS), the delay in the forced vibration state between the
589 rotation and the translation peaks is computed using the cross-correlation function available in
590 MatLab®. The results presented in Table 6 clearly confirm that a correlation exists between
591 these peaks. Only the smallest positive correlated delay is considered for each combination
592 because the peak in rotation was observed to almost always follow the peak in translation. The
593 average delays for the EW and NS directions are 0.47 and 0.25 s, respectively, with an average
594 standard deviation of 16% for both delays. The two distinct force-resisting mechanisms
595 associated with the RC cores might explain this significant difference for this building. The cores
596 resist the seismic forces as a ductile coupled system in the EW direction, whereas they act as
597 simple individual ductile walls in the NS direction. According to Table 6, the delay decreases for
598 most ground motions for larger B values. Thus, the SRFS and the torsional flexibility of the

building both have an effect on the delay. However, an exhaustive study including many SFRS and building geometries would be required to assess whether this conclusion can be generalized.

Table 6. Correlated delay (s) between peaks in rotation and in translation (at the top CM)

	B=1.7		B=2.1		B=2.5	
	EW	**NS**	**EW**	**NS**	**EW**	**NS**
GM1	0.43	0.10	0.29	0.13	0.22	0.13
GM2	0.60	0.13	0.29	0.13	0.16	0.11
GM3	0.47	0.12	0.35	0.14	0.35	0.18
GM4	0.60	0.31	0.45	0.16	0.41	0.20
GM5	0.48	0.15	0.41	0.15	0.39	0.14
GM6	0.61	0.18	0.56	0.15	0.51	0.13
GM7	0.46	0.12	0.20	0.09	0.20	0.06
GM8	0.72	0.14	0.66	0.26	0.47	0.19
GM9	0.44	0.13	0.31	0.13	0.27	0.12
GM10	0.70	0.70	0.72	0.73	0.70	0.68
GM11	0.53	0.15	0.36	0.09	0.29	0.08
GM12	0.71	0.66	0.67	0.32	0.54	0.17

5. Conclusions

A wide-column model (WCM) is used to assess the 3D nonlinear dynamic behavior of RC cores subjected to ground motions. This model consists of vertical fiber beam elements attached together with rigid horizontal links to ensure a uniform motion of the structure. The validity and robustness of the WCM were clearly demonstrated in this study through two validation cases, especially concerning the inelastic warping behavior due to torsion loads. By displacing the center of mass, three different building configurations with increasing torsional flexibility (B=1.7, B=2.1 and B=2.5 according to the NBCC 2010) were studied to investigate the effect of torsion on the seismic response. After validating the linear dynamic behavior, the WCM was

extended to three-dimensional nonlinear time history analyses of a multi-story building located in ENA. The main conclusions can be summarized as follows:

- The WCM can capture the inelastic warping behavior of open RC sections subjected to a monotonically increasing torque reasonably well. According to the experimental calibration, it is recommended that 25% of the initial elastic torsional stiffness (GJ) be assigned to the rigid links to achieve convergence with satisfactory results for cores subjected to high torsional loads. This value is also recommended in [12] for structures not subjected to significant torsion. Using higher values may lead to significant overestimation of the nonlinear torsional response of U-shaped RC structures.
- To provide a better representation of the behavior of open thin-walled RC structures, the number of modules of the WCM can be increased to enhance accuracy, but this might require a significantly larger computational time. When modeling RC cores subjected to dynamic loads, it is suggested that three modules (one per flange and one for the web) be used to ensure both precision and computational efficiency.
- A shell model is developed in ETABS 2015 to assess the linear dynamic behavior of the WCM. According to modal and linear time history analyses, the WCM can capture both translational and rotational modes of vibration with sufficient accuracy and can simulate the dynamic behavior of RC cores subjected to ground motions extremely well.
- The nonlinear results are compared to the design envelopes obtained from the response spectrum analysis of the linear shell model with proper code inelastic force reduction factors. These design envelopes exhibit very good agreement with the nonlinear response of the building if the A23.3-14 dynamic shear amplification factor is used to account for the inelastic effects of the higher modes. The computed rotations from the response

spectrum analysis are conservative, whereas the translational displacements are similar to the nonlinear envelopes. Large rotations are observed in the upper part of the cores because a low effective shear stiffness value was specified in the WCM to account for higher modes effects. Thus, this effective shear stiffness must be carefully selected if large rotational demands are expected, as is the case for torsionally flexible buildings. The shear and moment nonlinear envelopes remain relatively constant regardless of the B value. In contrast, the story torque increases as the building becomes more torsionally flexible.

- For the selected building, the rotation peaks almost always occur after the translation peaks. According to cross-correlation, this small delay (between 0.25 and 0.47 s) seems to be SFRS category dependent and it generally decreases for larger values of B.
- The proposed WCM fiber element approach is robust and computationally efficient. It represents a step toward characterizing the 3D nonlinear seismic response of RC cores subjected to significant torsional demand.

In the near future, the authors intend to conduct an extensive parametric seismic analysis of various building configurations using the WCM to define appropriate loading protocols including torsion. These loading protocols will be used to conduct large-scale cyclic biaxial tests of RC cores including significant torsion in the multi-directional (6 DOFs) testing facility of École Polytechnique de Montreal (EPM) [31].

6. Acknowledgements

The authors would like to acknowledge the financial contribution of the *Natural Sciences and Engineering Research Council of Canada* (NSRERC) and the *Fonds de recherche du Québec* -

Nature et technologie (FRQNT) to this project. The authors acknowledge thorough comments made by the reviewers. Those contributed significantly to the improvement of the paper.

7. References

[1] National Research Council of Canada. National Building Code of Canada. Ottawa, ON2010.
[2] American Society of Civil Engineers. Minimum Design Loads for Buildings and Other Structures (ASCE/SEI 7-10). Reston, VA.2010.
[3] Mazzoni S, McKenna F, Scott M, Fenves GL. OpenSees v2.4.4. Berkeley, CA: University of California; 2006.
[4] Humar J, Yavari S, Saatcioglu M. Design for forces induced by seismic torsion. Canadian Journal of Civil Engineering. 2003;30:328-37.
[5] Stafford-Smith B, Coull A. Tall building structures : analysis and design. New York, NY: John Wiley & Sons; 1991.
[6] Stafford-Smith B, Taranath BS. The analysis of tall core-supported structures subjected to torsion. ICE Proceedings: Thomas Telford; 1972. p. 173-87.
[7] Coull A, Chee WY. Stiffening of Structural Cores by Floor Slabs. Journal of Structural Engineering. 1986;112:977-94.
[8] Clough RW, King IP, Wilson EL. Structural analysis of multistory buildings. J Struct Div, ASCE. 1964;90:19-34.
[9] MacLeod IA. Analysis of shear wall buildings by the frame method. Proceedings of the Institution of Civil Engineers. 1973;55:593-603.
[10] Stafford Smith B, Abate A. Analysis of non-planar shear wall assemblies by analogous frame. ICE Proceedings: Thomas Telford; 1981. p. 395-406.
[11] Stafford Smith B, Girgis AM. Simple Analogous Frames for Shear Wall Analysis. Journal of Structural Engineering. 1984;110:2655-66.
[12] Beyer K, Dazio A, Priestley MJN. Inelastic wide-column models for U-shaped reinforced concrete walls. Journal of Earthquake Engineering. 2008;12:1-33.
[14] Beyer K, Dazio A, Priestley MJN. Quasi-Static Cyclic Tests of Two U-Shaped Reinforced Concrete Walls. Journal of Earthquake Engineering. 2008;12:1023-53.
[15] Stafford-Smith B, Girgis AM. Deficiencies in the Wide Column Analogy for Shear Wall Core Analysis. Concrete International. 1986;8:58-61.
[16] Kwan AKH. Improved Wide-Column-Frame Analogy for Shear/Core wall Analysis. Journal of Structural Engineering. 1993;119:420-37.
[17] Scott BD, Park R, Priestley MJN. Stress-Strain Behavior of Concrete Confined by Overlapping Hoops at Low and High Strain Rates. ACI Journal Proceedings. 1982;79:13-27.
[18] Beyer K, Dazio A, Priestley MJN. Shear Deformations of Slender Reinforced Concrete Walls under Seismic Loading. ACI Structural Journal. 2011;108:167-77.
[19] Krpan P, Collins MP. Testing Thin-Walled Open RC Structure in Torsion. Journal of the Structural Division. 1981;107:1129-40.
[20] SIMULIA DS. ABAQUS. 6.11 ed. Providence, RI: DS SIMULIA Corp.; 2011.
[21] CSA. Design of concrete structures. Rexdale, ON: Canadian Standards Association; 2014.
[22] Stafford-Smith, B., & Coull, A.Tall building structures: analysis and design. John Wiley & Sons.1991.
[23] Ben Ftima M., Massicotte B. Utilization of Nonlinear Finite Elements for the Design and Assessment of Large Concrete Structures. I: Calibration and Validation. Journal of Structural Engineering. 2014.
[24] National Research Council of Canada. National Building Code of Canada. Ottawa, ON2005.
[25] CSA. Design of concrete structures. Rexdale, ON: Canadian Standards Association; 2004.

706 [26] CAC. Concrete Design Handbook. 3 ed. Ottawa, ON: Cement Association of Canada (CAC); 2010.
707 [27] CSI. ETABS. 15.0.0 ed. Berkeley, CA: Computers and Structures inc.; 2015.
708 [28] Luu H, Ghorbanirenani I, Léger P, Tremblay R. Numerical modeling of slender reinforced concrete
709 shear wall shaking table tests under high-frequency ground motions. Journal of Earthquake Engineering.
710 2013;17:517-42.
711 [29] Luu H, Léger P, Tremblay R. Seismic demand of moderately ductile reinforced concrete shear walls
712 subjected to high-frequency ground motions. Canadian Journal of Civil Engineering. 2013;41:125-35.
713 [29] Charney FA. Unintended consequences of modeling damping in structures. Journal of structural
714 engineering. 2008;134:581-92.
715 [30] Pelletier K. Considération de la torsion pour l'analyse sismique non-linéaire de noyaux en béton
716 armé. QC, Canada: École Polytechnique de Montréal; 2015.
717 [31] Tremblay R, Léger P, Rogers C, Bouaanani N, Massicotte B, Khaled A et al. Experimental Testing
718 of Large Scale Structural Models and Components Using Innovative Shake Table Dynamic, Real time
719 hybrid simulation and multidirectional loading techniques. Proc 3rd Int Conf on Advances in
720 Experimental Structural Engineering. San-Francisco, USA2009. p. 1-12.
721

722

723 **Figure Captions**

724

725 Fig. 1. Core wall in a reinforced concrete structure

726 Fig. 2. Definition of e_x and D_{nx}

727 Fig. 3. (a) Planar shear wall and (b) wide-column analogy

728 Fig. 4. Shear behavior of a core structure: (a) shear stresses, (b) WCM representation and (c)

729 additional shear deformations

730 Fig. 5. WCM model with modules: (a) 3D view and (b) cross-sectional view (m=6)

731 Fig. 6. T-θ relationship of the Krpan and Collins (1981) experiment

732 Fig. 7. Deformed ABAQUS model at failure: (a) concrete cracking damage indicator (d=1 for

733 complete cracking) and (b) reinforcement stresses in MPa (positive in tension)

734 Fig. 8. Sensitivity analyses of rigid links: (a) Saint-Venant stiffness for m=3 and (b) spacing for

735 m=9

736 Fig. 9. Beyer et al. (2008) experiment: (a) test setup [13] and (b) loading history [12]

737 (reproduced with the permission of Taylor and Francis Ltd)

738 Fig. 10. TUA hystereses (Beyer et al. [12] results reproduced with the permission of Taylor and

739 Francis Ltd)

740 Fig. 11. Plan view of the selected building

741 Fig. 12. Linear time history response to GM1 in the NS direction (with A23.3-04 stiffness

742 reduction factors)

743 Fig. 13. Nonlinear time history response to GM1 in the NS direction

744 Fig. 14. Displacement and rotation envelopes in the NS direction

745 Fig. 15. Force and moment envelopes in the NS direction (DSA and design curves correspond to
746 the 2005 design values with and without dynamic shear amplification)
747
748
749
750

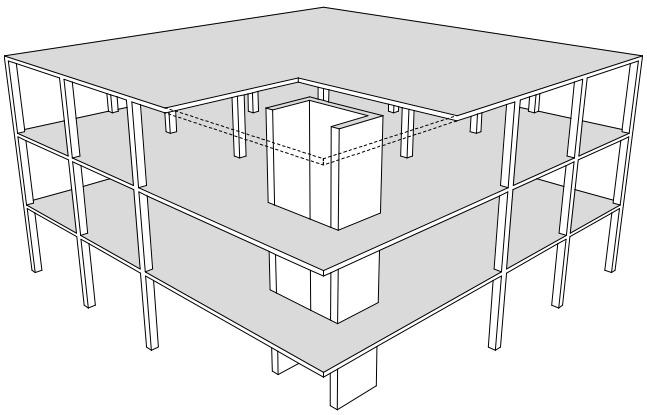

Fig. 1. Core wall in a reinforced concrete structure

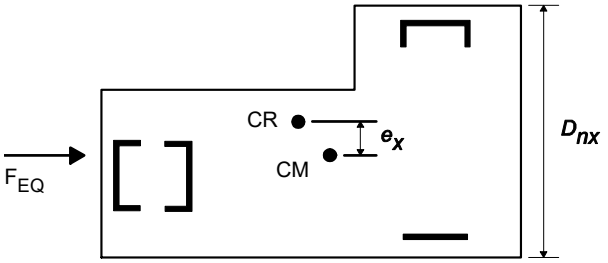

Fig. 2. Definition of e_x and D_{nx}

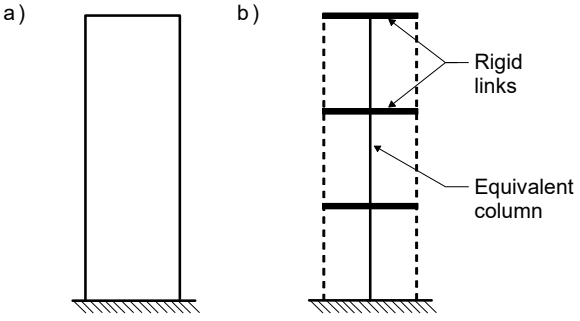

Fig. 3. (a) Planar shear wall and (b) wide-column analogy

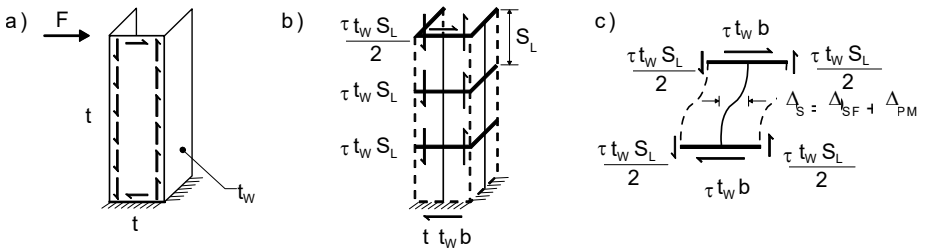

10

11 Fig. 4. Shear behavior of a core structure: (a) shear stresses, (b) WCM representation and (c)

12 additional shear deformations

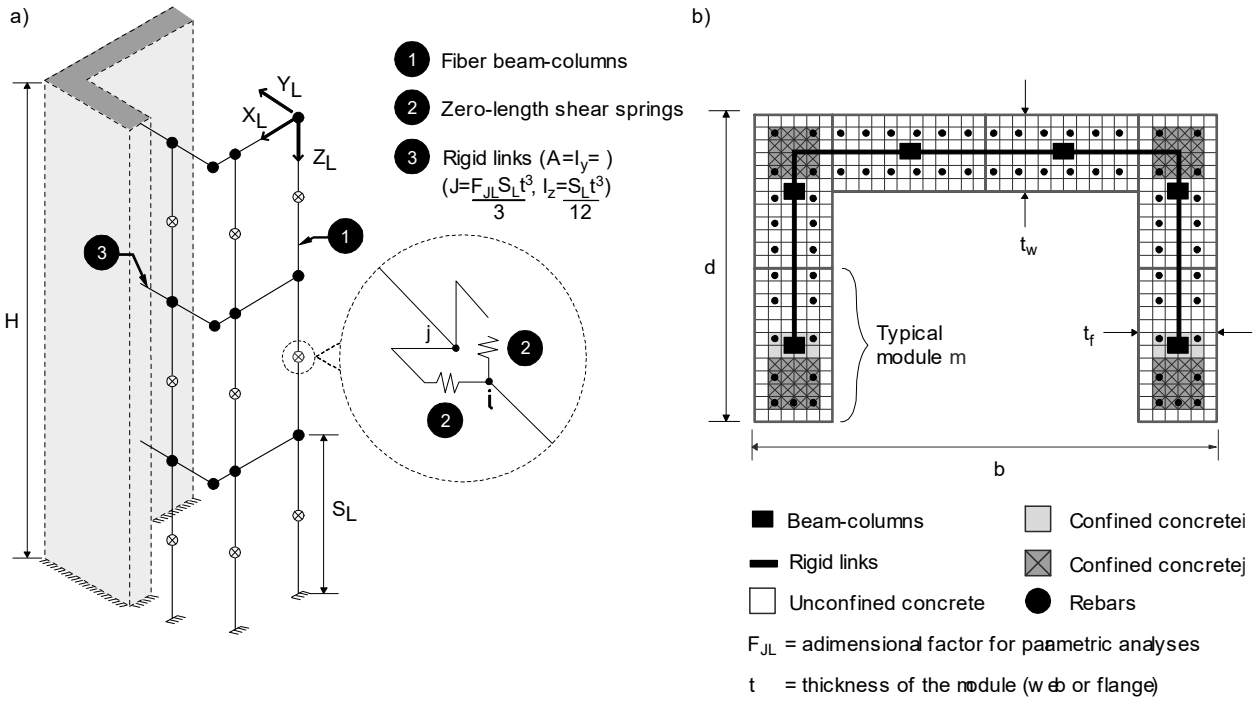

13

14 Fig. 5. WCM model with modules: (a) 3D view and (b) cross-sectional view (m=6)

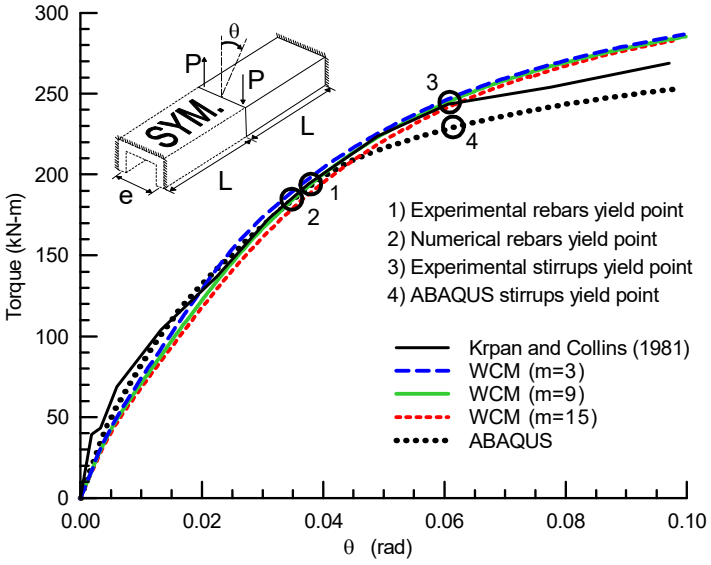

15

16 Fig. 6. T-θ relationship of the Krpan and Collins (1981) experiment

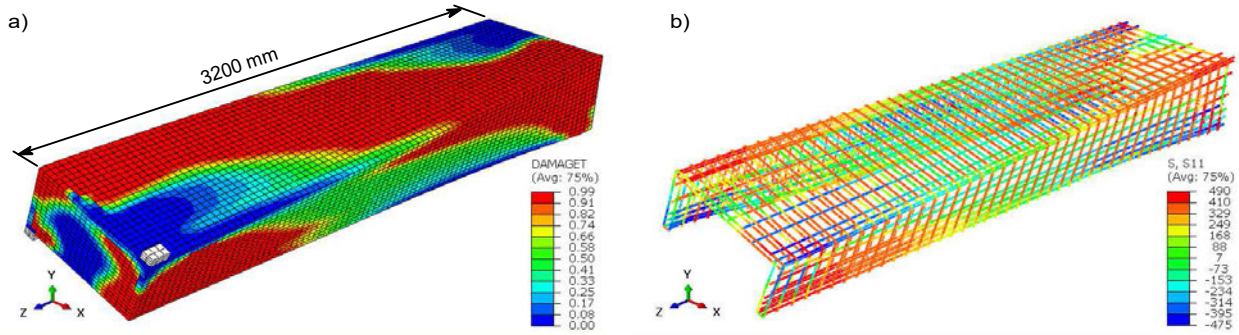

17

18 Fig. 7. Deformed ABAQUS model at failure: (a) concrete cracking damage indicator (d=1 for

19 complete cracking) and (b) reinforcement stresses in MPa (positive in tension)

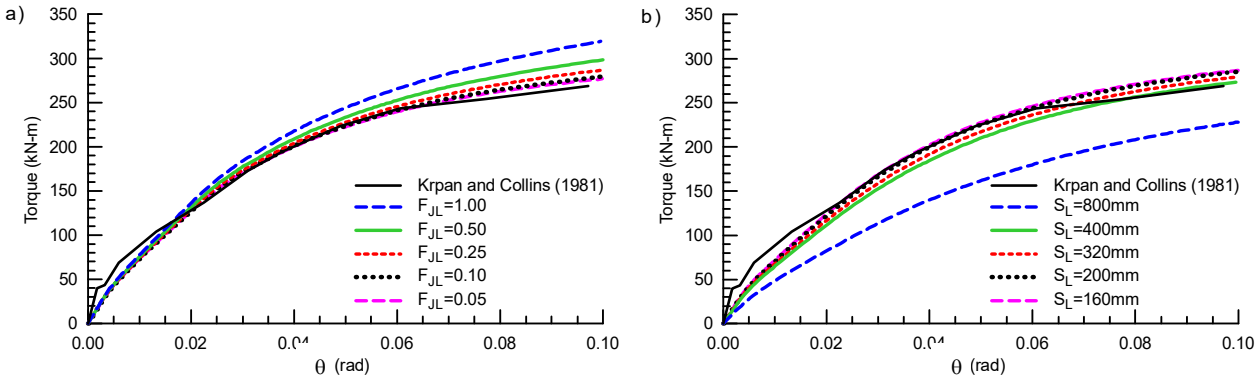

20

21 Fig. 8. Sensitivity analyses of rigid links: (a) Saint-Venant stiffness for m=3 and (b) spacing for

22 m=9

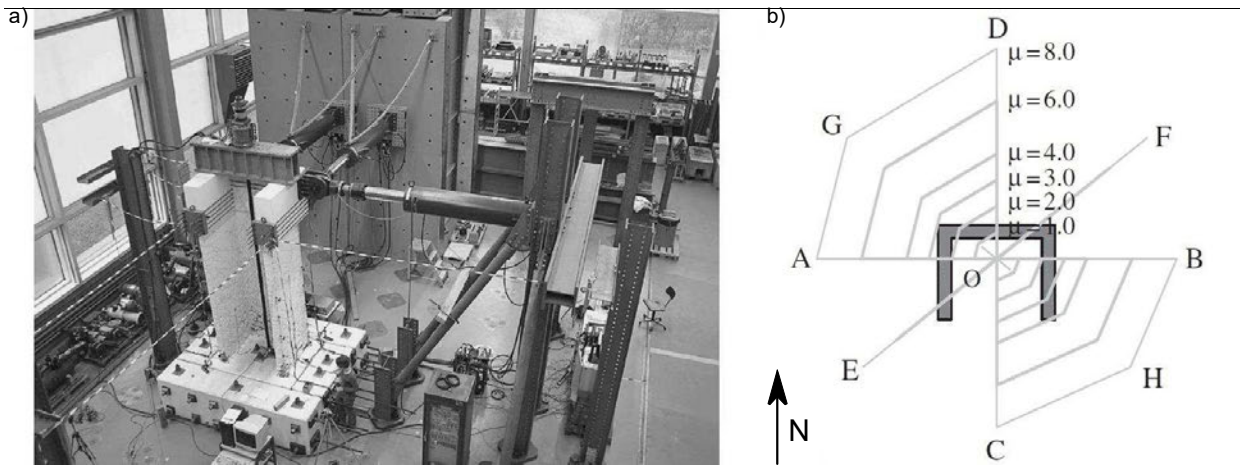

Fig. 9. Beyer et al. (2008) experiment: (a) test setup [13] and (b) loading history [12] (reproduced with the permission of Taylor and Francis Ltd)

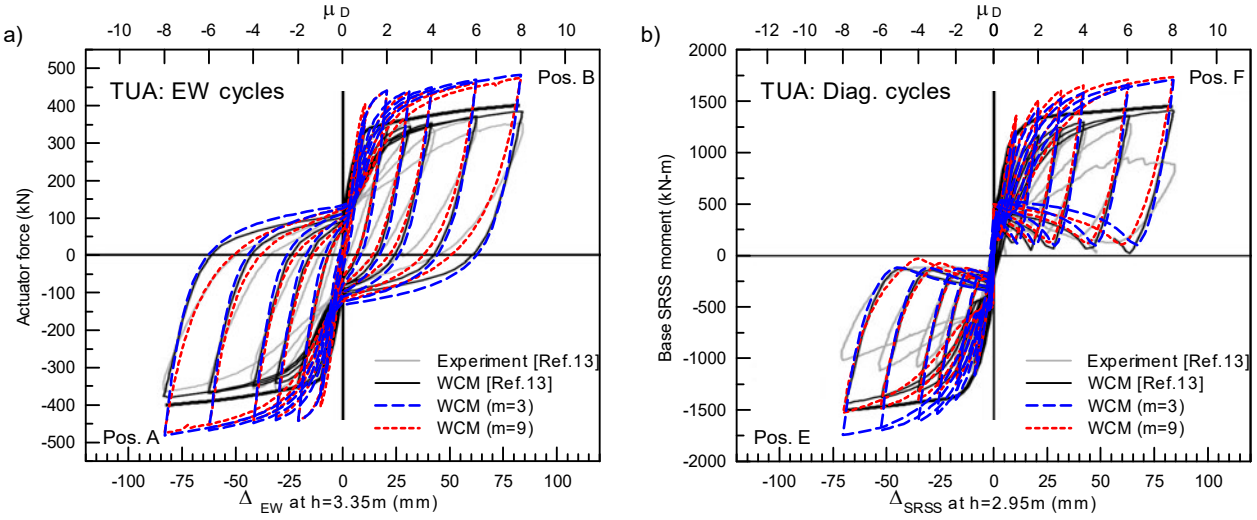

Fig. 10. TUA hystereses (Beyer et al. [12] results reproduced with the permission of Taylor and Francis Ltd)

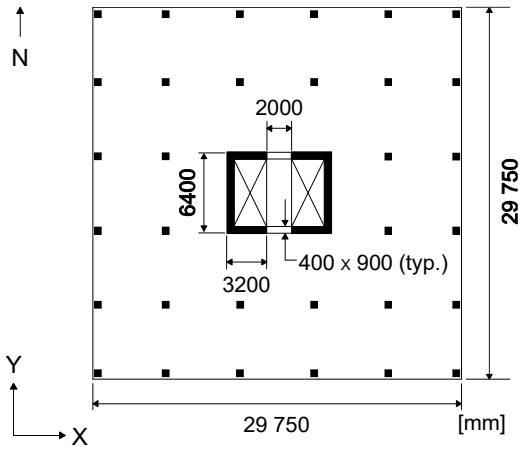

Material properties

f'_c = 30 MPa
f'_t = 3.29 MPa
E_c = 24 650 MPa
F_y = 400 MPa
E_s = 200 000 MPa

Fig. 11. Plan view of the selected building

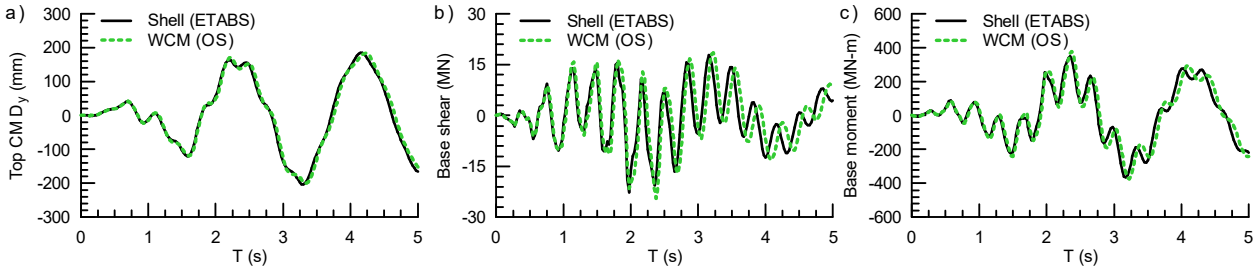

Fig. 12. Linear time history response to GM1 in the NS direction (with A23.3-04 stiffness reduction factors)

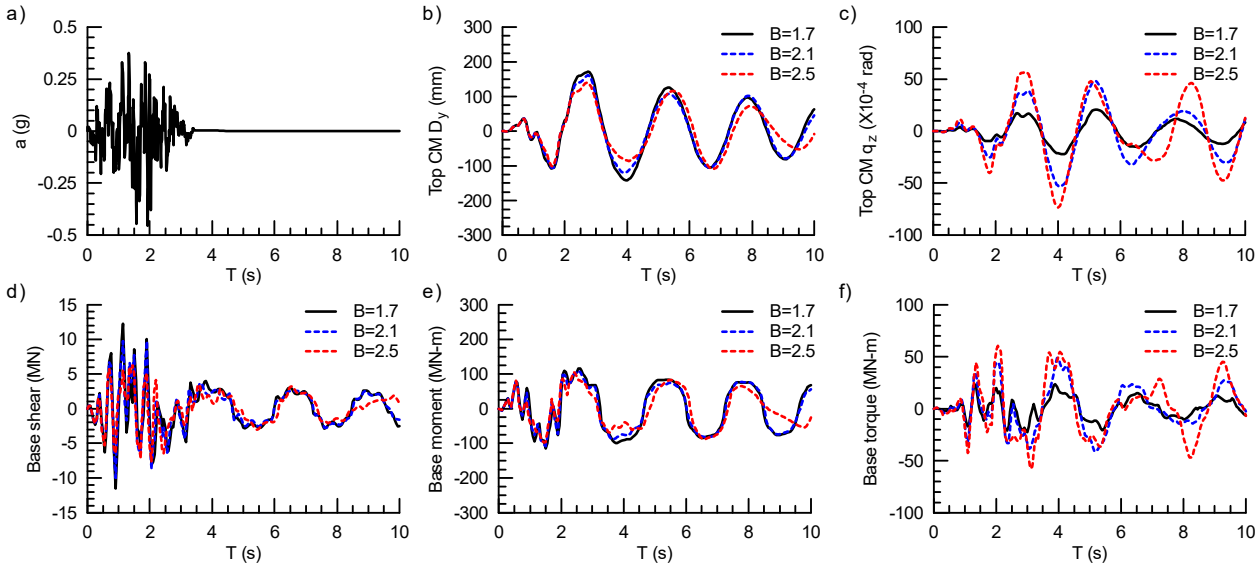

37

38 Fig. 13. Nonlinear time history response to GM1 in the NS direction

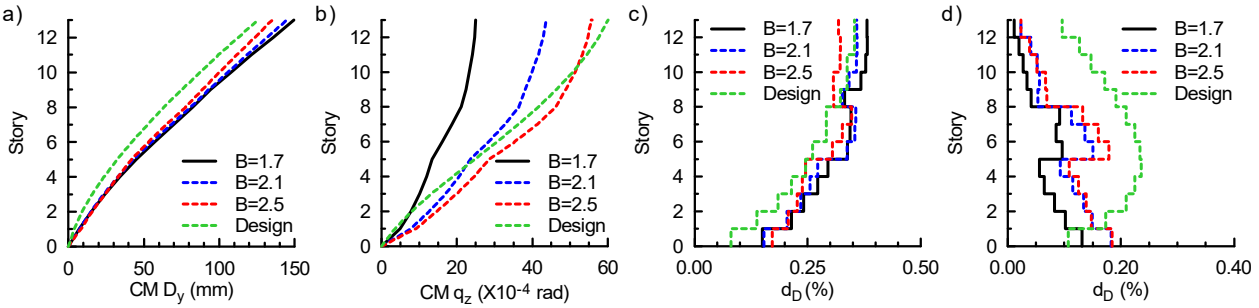

39

40 Fig. 14. Displacement and rotation envelopes in the NS direction

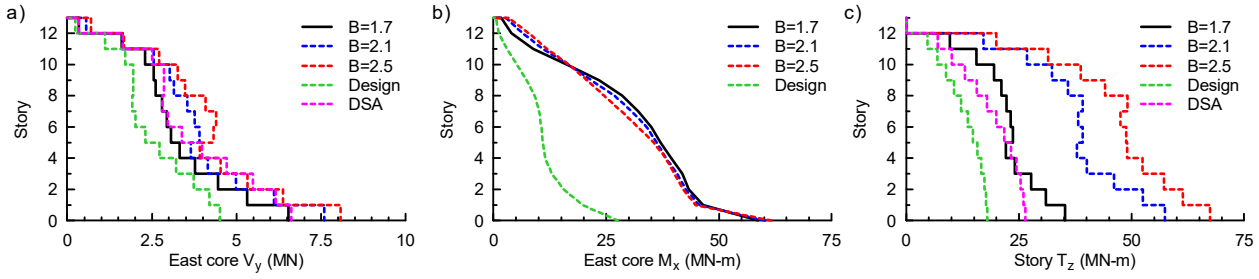

41

42 Fig. 15. Force and moment envelopes in the NS direction (DSA and design curves correspond to

43 the 2005 design values with and without dynamic shear amplification)

44

45

46